Received: 27 March 2023 | Accepted: 8 September 2023

DOI: 10.1097/HEP.0000000000000637

ORIGINAL ARTICLE

A genetic basis of mitochondrial *DNAJA3* in nonalcoholic steatohepatitis-related hepatocellular carcinoma

Ching-Wen Chang[1,2,3] | Yu-Syuan Chen[2] | Chen-Hua Huang[4] | Chao-Hsiung Lin[4] | Wailap Victor Ng[5,6] | Lichieh Julie Chu[7,8,9] | Eric Trépo[10,11,12] | Jessica Zucman-Rossi[10,13] | Kevin Siao[14] | Jacquelyn J. Maher[14] | Men Yee Chiew[15] | Chih-Hung Chou[15,16] | Hsien-Da Huang[15,17,18] | Wan-Huai Teo[2] | I-Shan Lee[2] | Jeng-Fan Lo[2,19,20] | Xin Wei Wang[1,21]

[1]Laboratory of Human Carcinogenesis, Center for Cancer Research, National Cancer Institute, National Institutes of Health, Bethesda, Maryland, USA

[2]Institute of Oral Biology, School of Dentistry, National Yang Ming Chiao Tung University, Taipei, Taiwan

[3]Graduate Institute of Metabolism and Obesity Sciences, College of Nutrition, Taipei Medical University, Taipei, Taiwan

[4]Department of Life Sciences and Institute of Genome Sciences, National Yang Ming Chiao Tung University, Taipei, Taiwan

[5]Department of Biotechnology and Lab Science in Medicine, National Yang Ming Chiao Tung University, Taipei, Taiwan

[6]Department of Biochemistry, Kaohsiung Medical University, Kaohsiung, Taiwan

[7]Graduate Institute of Biomedical Sciences, College of Medicine, Chang Gung University, Taoyuan, Taiwan

[8]Molecular Medicine Research Center, College of Medicine, Chang Gung University, Taoyuan, Taiwan

[9]Department of Otolaryngology - Head & Neck Surgery, Chang Gung Memorial Hospital, Linkou, Taiwan

[10]Centre de Recherche des Cordeliers, Sorbonne Université, Université de Paris, INSERM, Paris, France

[11]Department of Gastroenterology, Hepatopancreatology and Digestive Oncology, CUB Hôpital Erasme, Université Libre de Bruxelles, Brussels, Belgium

[12]Laboratory of Experimental Gastroenterology, Faculty of Medicine, Université Libre de Bruxelles, Brussels, Belgium

[13]Assistance Publique Hôpitaux de Paris, Hôpital Européen Georges Pompidou, Département d′Oncologie, Paris, France

[14]Department of Medicine, Liver Center, University of California, San Francisco, California, USA

[15]Department of Biological Science and Technology, National Yang Ming Chiao Tung University, Hsinchu City, Taiwan

[16]Department of Biological Science and Technology, Center for Intelligent Drug Systems and Smart Bio-devices, National Yang Ming Chiao Tung University, Hsinchu City, Taiwan

[17]School of Life and Health Sciences, The Chinese University of Hong Kong, Shenzhen, Longgang District, Shenzhen, China

[18]Warshel Institute for Computational Biology, School of Medicine, Life and Health Sciences, The Chinese University of Hong Kong, Shenzhen, Longgang District, Shenzhen, China

[19]Cancer Progression Research Center, National Yang Ming Chiao Tung University, Taipei, Taiwan

[20]Department of Dentistry, Taipei Veterans General Hospital, Taipei, Taiwan

[21]Liver Cancer Program, Center for Cancer Research, National Cancer Institute, National Institutes of Health, Bethesda, Maryland, USA

Correspondence
Xin Wei Wang, Laboratory of Human Carcinogenesis, Center for Cancer Research, National Cancer Institute, National Institutes of Health, 37 Convent Drive, Building 37, Room 3044A, Bethesda, MD 20892, USA.
Email: xw3u@nih.gov

Abstract

Background and Aims: NAFLD is the most common form of liver disease worldwide, but only a subset of individuals with NAFLD may progress to NASH. While NASH is an important etiology of HCC, the underlying

Abbreviations: DNAJA3, DnaJ Heat Shock Protein Family (Hsp40) Member A3; DEN, diethylnitrosamine; eQTL, expression quantitative trait loci; FAO, fatty acid oxidation; HFD, high-fat diet; OXPHOS, oxidative phosphorylation.

Ching-Wen Chang and Yu-Syuan Chen contributed equally to this work.

Supplemental Digital Content is available for this article. Direct URL citations are provided in the HTML and PDF versions of this article on the journal's website, www.hepjournal.com.

Jeng-Fan Lo, Institute of Oral Biology, National Yang Ming Chiao Tung University, Taipei 112304, Taiwan. Email: iflo@nycu.edu.tw

mechanisms responsible for the conversion of NAFLD to NASH and then to HCC are poorly understood. We aimed to identify genetic risk genes that drive NASH and NASH-related HCC.

Approach and Results: We searched genetic alleles among the 24 most significant alleles associated with body fat distribution from a genome-wide association study of 344,369 individuals and validated the top allele in 3 independent cohorts of American and European patients (N = 1380) with NAFLD/NASH/HCC. We identified an rs3747579-TT variant significantly associated with NASH-related HCC and demonstrated that rs3747579 is expression quantitative trait loci of a mitochondrial DnaJ Heat Shock Protein Family (Hsp40) Member A3 (*DNAJA3*). We also found that rs3747579-TT and a previously identified *PNPLA3* as a functional variant of NAFLD to have significant additional interactions with NASH/HCC risk. Patients with HCC with rs3747579-TT had a reduced expression of *DNAJA3* and had an unfavorable prognosis. Furthermore, mice with hepatocyte-specific *Dnaja3* depletion developed NASH-dependent HCC either spontaneously under a normal diet or enhanced by diethylnitrosamine. *Dnaja3*-deficient mice developed NASH/HCC characterized by significant mitochondrial dysfunction, which was accompanied by excessive lipid accumulation and inflammatory responses. The molecular features of NASH/HCC in the *Dnaja3*-deficient mice were closely associated with human NASH/HCC.

Conclusions: We uncovered a genetic basis of *DNAJA3* as a key player of NASH-related HCC.

INTRODUCTION

Liver cancer is the third deadliest cancer, and HCC is the main liver cancer type.[1] In recent years, HCC incidence continues to rise globally, despite our ability to effectively prevent HBV-related or HCV-related HCC.[2] Changing trends in etiologies such as diet-related liver diseases may contribute to the rising incidence. For example, unhealthy diets may induce NAFLD, which affects approximately 25% of the world's population. However, only 1 in 5 individuals with NAFLD progress to NASH, with some advancing to liver cirrhosis.[3] Individuals with metabolic syndrome–associated NASH have a high risk of developing HCC, which may contribute to the rising incidence of HCC in the United States.[4] The genetic basis for what drives the transition of NAFLD to NASH and then to HCC is unknown.

Several recent prospective cohort studies, including familial aggregation and twin studies, have provided strong evidence that NAFLD/NASH are heritable traits.[5,6] Subsequent epidemiological and genome-wide association studies linked several candidate genetic variants to NAFLD.[7,8] One variant, PNPLA3 I148M, has been shown as a significant genetic risk factor of NAFLD by altering lipid droplet dynamics.[9] Yet, the existing risk variants account for only a fraction of NASH/HCC heritability, highlighting the paradox that while not every individuals with obesity or NAFLD develops NASH, some individuals without obesity do.[10] The key question remains as to why only some of the individuals with NAFLD-related variants will progress from NAFLD to NASH and then HCC. Crucially, several studies pinpoint regional body fat distribution, even when adjusted for body mass index, as an inheritable risk for detrimental metabolic outcomes.[11–13] This distribution is intertwined with metabolic syndrome, playing a pivotal role in NASH/HCC development.[14–16] Thus, we hypothesized that some of the body fat distribution–associated genetic variants may be linked to the risk of NASH/HCC.

Here, by searching a database of body fat distribution–related variants[13] to be associated with NASH-related HCC and by generating a genetically engineered mouse model, we aimed to determine genes that drive NASH and NASH-related HCC. We identified a genetic variant rs3747579 linked to the reduced expression of mitochondrial chaperone Hsp40, also known as DnaJ Heat Shock Protein Family

(Hsp40) Member A3 (*DNAJA3*),[17] and its association with NASH-related HCC. Experimentally, mice with hepatocyte-specific deletions of *Dnaja3* developed NASH and HCC. Mice with *Dnaja3* ablation progressively developed fatty liver, NASH, and cirrhosis/HCC phenotypes. We also demonstrated that hepatic *Dnaja3* deficiency impaired mitochondrial function in hepatocytes, which led to compensatory excessive lipid accumulation, resulting in inflammation and tumor progression. Our results may provide a genetic basis of *DNAJA3*, which may be useful as a risk marker for NASH, and that *DNAJA3*-mediated signaling may be therapeutically exploited for NASH-related HCC.

METHODS

National Cancer Institute - University of Maryland (NCI-UMD) cohort

The demographic characteristics of participant groups of the National Cancer Institute - University of Maryland (NCI-UMD) cohort are summarized in Supplemental Tables S1, http://links.lww.com/HEP/I71 and S2, http://links.lww.com/HEP/I71. All clinic measurements of the NCI-UMD cohort were covered by NCT00913757 (clinicaltrials.gov) as described.[18] Serum, whole blood, plasma, or cheek swabs were collected at the time of the interview. Sera and saliva were stored at −80 °C for research. The study was approved by the NCI Institutional Review Boards. All participants provided written informed consent as described.[18]

Animal care and generation of *Dnaja3*$^{-/-}$ mice

All animal work was approved by the Institutional Animal Care and Use Committee (IACUC) and conducted according to guidelines established. We used the ARRIVE reporting guidelines.[19] The details of the generation of *Dnaja3*$^{flx/flx}$ mice on a C57BL/6N background were available in Supplemental Methods, http://links.lww.com/HEP/I70. Liver-specific *Dnaja3*$^{-/-}$ (albumin-Cre; *Dnaja3*$^{flx/flx}$) mice were generated by crossing *Dnaja3* floxed (*Dnaja3*$^{flx/flx}$) mice with Albumin-Cre mice (a gift from Dr. Ann-Ping Tsou, National Yang Ming Chiao Tung University). *Dnaja3*$^{-/-}$ and *Dnaja3*$^{flx/flx}$ mice were littermates. Mice were killed at a time point indicated in the figure legends using CO_2 euthanasia, and blood and tissue samples were harvested for morphological, biochemical, and functional measurements. If mice showed severe weakness or 20% weight loss, mice were euthanized with CO_2. Mice numbers of 5 were used unless stated. All mice used were males unless stated. The age and sex of the mice were indicated in the figure legends. The details for the generation of animal models and treatments, as well as other experimental protocols, are available in Supplemental Methods, http://links.lww.com/HEP/I70.

RESULTS

Identification of the *DNAJA3* rs3747579-TT variant linked to NASH and HCC

Using the Illumina OmniExpress single nucleotide polymorphism (SNP) array to analyze the NCI-UMD case-control cohort,[18] which includes 484 healthy volunteers, 499 individuals without NASH (non-NASH, either with chronic liver diseases due to other etiologies or with HCC), and 26 individuals with confirmed NASH (including at-risk and HCC) (Figure 1A, Supplemental Tables S1, http://links.lww.com/HEP/I71 and S2, http://links.lww.com/HEP/I71), we identified the association of 24 SNPs between the individuals with and without NASH from the NCI-UMD cohorts. Among these, 4 coding variants (rs3747579, rs8052655, rs3764002, and rs897453) had a Bonferroni-corrected *p*-value, with rs3747579 showing the strongest association in 4 genetic models (codominant, dominant, recessive, and log-additive models) (Figure 1B and Supplemental Figure S1A, http://links.lww.com/HEP/I72). The associations were assessed using the max-statistic or standard statistic (Supplemental Tables S5 and S6, http://links.lww.com/HEP/I71). The significance persisted after adjusting for age and sex (Supplemental Table S7, http://links.lww.com/HEP/I71). Among the 4 NASH-associated variants, rs897453 was a strong expression quantitative trait loci (eQTL) for *PEMT* (Supplemental Table S5, http://links.lww.com/HEP/I71), which is a hepatic integral membrane protein localized to the endoplasmic reticulum and a risk allele for lean NASH.[20] In addition, rs3764002 was a eQTL for *CMKLR1* known to be associated with protection against NASH.[21] These results provide further confidence in our initial approach. We focused on rs3747579 as it had the strongest association. We found that rs3747579-TT was significantly associated with NASH with OR of 16.1 (95% CI: 2.0–128.3; $p = 1E-03$) (Supplemental Figure S1B, http://links.lww.com/HEP/I72 and Supplemental Table S8, http://links.lww.com/HEP/I71). Furthermore, rs3747579-TT was associated with NASH in the University of California, San Francisco cohort with a similar trend, but it was statistically no significant; some comparisons were limited by available data and therefore may not have been adequately powered to detect meaningful differences (Supplemental Table S9, http://links.lww.com/HEP/I71). We then combined both NCI-UMD cohort and University of California, San Francisco cohort as the US cohort and found consistent data that rs3747579-TT was associated with NASH ($p = 7E-04$) (Supplemental Table S10, http://links.lww.com/HEP/I71). We also examined a

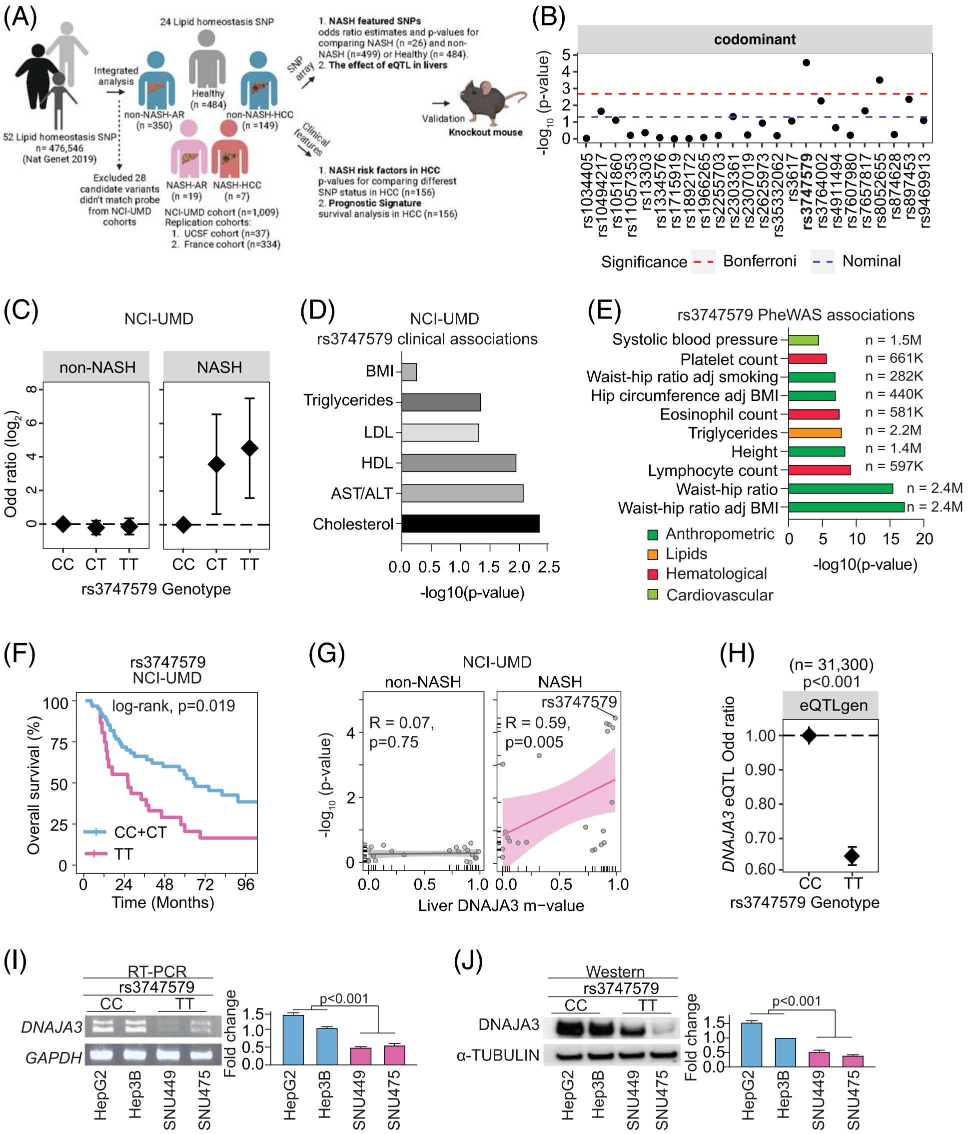

FIGURE 1 Identification of candidate genes for NASH and NASH-related HCC risk variants. (A) Schema of an integrated analysis of lipid homeostasis SNP (Nat Gent, 2019) and NASH risk. The NASH risk effect of allele observed from NASH disease cases (n = 26), including AR of NASH (NASH-AR, n = 19) and NASH-related HCC (NASH-HCC, n = 7) individuals compared with population controls (PC, n = 484) or chronic or alcohol-associated liver disease cases (non-NASH, n = 499) including individuals at risk (non-NASH-AR, n = 350) and with HCC (non-NASH-HCC, n = 149). In addition, to determine the nature of the relationship between lipid homeostasis SNPs and the clinicopathological characteristics of NASH-related HCC, patients with HCC (n = 156) were divided into subgroups according to lipid homeostasis SNP status to character the NASH feature, such as cholesterol; the resulting were validated in *Dnaja3* knockout mice. (B) Manhattan plot based on the dominant genetic model for the association of NASH-related HCC risk coding variants that overlapped with 24 common variants of lipid homeostasis. Red dotted line indicates the threshold for NASH group (n = 26) compared with non-NASH group (n = 499) after the Bonferroni correction. Blue dotted line shows the nominal level of significance. (C) ORs and 95% CIs of rs3747579 genotype among non-NASH (n = 499) or NASH (n = 26) relative to the control (n = 484) group. Further details are available in Supplemental Table S8, http://links.lww.com/HEP/I71. (D) The associations between rs3747579 and NASH clinical features. The box plot shows −log10 (*p*-values) based on the effect of the different rs3747579 genotypes in the HCC samples (n = 156). Further details are available in Supplemental Table S14, http://links.lww.com/HEP/I71. (E) The PheWAS plot shows the top 10 significant associations of rs3747579 for all available traits in the Common Metabolic Diseases Knowledge Portal, generated by bottom-line meta-analysis across all data sets. n refers to sample size. (F) Kaplan-Meier curves for the overall survival according to the rs3747579 genotype of patients with HCC from UMD (CC+CT: n = 60; TT: n = 28) cohort adjusting for age, sex, and race/ethnicity. (G) Scatter plot of the NASH-specific eQTL association between each SNP's genotype and *DNAJA3* m-value in the liver from the GTEx database (n = 208). The *p*-values display an association with disease featural phenotype of the NCI-UMD cohort among non-NASH (n = 499) (left panel) and NASH group (n = 26) (right panel) relative to the control (n = 484) group. Each dot represents an eQTL of *DNAJA3* (n = 21). The m-value indicates the posterior probability that the eQTL affects expression in liver tissue. The eQTL affects expression in liver tissue if the m-value is ≥ 0.9. Further details are available in Table S15, http://links.lww.com/HEP/I71. (H) ORs and 95% CIs of *DNAJA3* expression among rs3747579 genotype. Summary statistics of *DNAJA3* eQTL was obtained from the IEU OpenGWAS (n = 31,300). (I) RT-PCR analysis of relative mRNA expression of *DNAJA3* gene in liver cancer cell lines carrying different rs3747579 genotypes. Data were first normalized to GAPDH to get ΔCt. Relative mRNA was then calculated by 2(−ΔCt). (J) Immunoblots showing DNAJA3 and α-Tubulin protein levels in liver cancer cell lines with different rs3747579 genotypes. Data are represented as mean ± SD. Abbreviations: ALT, alanine aminotransferase; AR, at-risk; AST, aspartate aminotransferase; BMI, body mass index; DNAJA3, DnaJ Heat Shock Protein Family (Hsp40) Member A3; eQTL, expression quantitative trait loci; GAPDH, glyceraldehyde 3-phosphate dehydrogenase; NCI-UMD, National Cancer Institute-University of Maryland; PheWAS, phenome-wide association studies; RT-PCR, reverse transcription polymerase chain reaction; SNP, single nucleotide polymorphism; UCSF, University of California, San Francisco.

French-Belgian cohort of 334 patients with NAFLD to further determine whether rs3747579-TT is associated with NAFLD/NASH-related HCC and found consistent results (Supplemental Table S11, http://links.lww.com/HEP/I71). Noticeably, rs3747579-TT was also significantly associated with HCC (OR: 2.14; $p = 4.9E\text{-}03$) (Supplemental Table S12, http://links.lww.com/HEP/I71). Collectively, these data indicate that rs3747579-TT may be linked to NASH and HCC.

We further compared the strength of association between rs3747579-TT and NASH with reported functional SNPs of *PNPLA3* and *TM6SF2*[22] to be linked to NAFLD in the NCI-UMD cohort. The rs3747579-TT significance persisted in NASH-HCC after adjusting for genetic variants of *PNPLA3* and *TM6SF2* (Supplemental Table S13, http://links.lww.com/HEP/I71). We also included data in all 24 lipid homeostasis–related SNPs for comparison, and again, rs3747579-TT had the strongest association independent of *PNPLA3* and *TM6SF2* (Supplemental Table S13, http://links.lww.com/HEP/I71). Noticeably, rs3747579 and genetic variants of *PNPLA3* showed highly significant additional interactions with NASH-HCC risk (Supplemental Figure S1C, http://links.lww.com/HEP/I72). The rs3747579-TT was also significantly associated with pathological and clinical features of NASH, for example, increased cholesterol and triglycerides in the NCI-UMD cohort (Figure 1D and Supplemental Table S14, http://links.lww.com/HEP/I71). Using phenome-wide association studies, we identified waist-hip ratio, triglyceride levels, and blood counts as significant features correlated with rs3747579 (Figure 1E).

To understand if rs3747579-TT was associated with a subgroup of HCC with different tumor biology, we examined the overall survival of patients with HCC based on the rs3747579 genotype status in the NCI-UMD cohorts. We found that the overall survival time of patients with HCC with rs3747579-TT was significantly shorter than that of those with CC and CT alleles in UMD-NCI cohort after adjusting for age, sex, and race/ethnicity (Figure 1F). Noticeably, we found similar results when the analysis was restricted to the Caucasian ancestry in both UMD-NCI and TCGA cohorts (Supplemental Figure S2A, http://links.lww.com/HEP/I72). We could not evaluate Black ancestry separately in the UMD-NCI cohort since cases with rs3747579-TT were not included. While the TCGA cohort also included Asian ancestry, we did not find a significant survival association linked to rs3747579-TT in Asian patients with HCC (Supplemental Figure S2B, http://links.lww.com/HEP/I72).

We performed eQTL analysis located upstream of the rs3747579 locus using the GTEX-Liver and TCGA-LIHC data sets. Intriguingly, despite its location in exon 7 of the *CORO7* gene, rs3747579 exhibited a pronounced association with *DNAJA3* expressions compared to *CORO7* (Supplemental Figure S3A, http://links.lww.com/HEP/I72). Moreover, we found that rs3747579-TT was significantly associated with decreased expression of *DNAJA3*, but not *CORO7*, compared to rs3747579-CC or CT allele in TCGA-LIHC cohorts (Supplemental Figure S3B, http://links.lww.com/HEP/I72). Furthermore, using the human protein atlas database,[23] we found that *DNAJA3*, but not *CORO7*, is highly expressed in the liver and in hepatocytes (Supplemental Figure S3C, D, http://links.lww.com/HEP/I72). Taken together, we concluded that rs3747579 is an eQTL linked to *DNAJA3* expression rather than *CORO7*.

We further explored the influence of rs3747579 on *DNAJA3* expression in NASH-related characteristics in the UMD-NCI cohorts. These SNPs were located within a 100-kb region upstream of the *DNAJA3* transcription start site and mapped to eQTL using data from the GTEx-liver cohort. We found a positive association between the m-value of *DNAJA3*-related eQTL and NASH-HCC but not with non-NASH-related features (Figure 1G). Consistently, rs3747579 in *DNAJA3* eQTL had the strongest association with NASH-HCC (Figure 1G and Supplemental Table S15, http://links.lww.com/HEP/I71). Moreover, a large eQTL database (eQTLgene) confirmed that the expression pattern of *DNAJA3* is dependent on the rs3747579 genotype (Figure 1H). To further determine whether *DNAJA3* rs3747579-TT is a bona fide allele linked to *DNAJA3* expression in hepatoma cells, we searched the CCLE database for rs3747579 variants in liver cell lines[24] that are available in our cell repository. We found and validated rs3747579-CC in HepG2 and Hep3B, and rs3747579-TT in SNU449 and SNU475 (Supplemental Figure S4A, B, http://links.lww.com/HEP/I72). We confirmed that the mRNA and protein levels of DNAJA3 were significantly lower in cells with the TT allele compared to the CC allele (Figure 1I, J). Similar results were obtained when assessing HCC cell lines that mimic the NASH phenotype (Supplemental Figure S4C, http://links.lww.com/HEP/I72). To assess if SNP rs3747579 affects transcription factor binding sites, we probed RegulomeDB for REMs within its genomic region. Chip-seq analysis revealed that rs3747579-CC variant is a part of a binding site of *RBFOX2* (Supplemental Figure S5A, http://links.lww.com/HEP/I72), a transcriptional activator and regulates cholesterol homeostasis.[25] Cells with *RBFOX2* knockdown displayed considerably lower *DNAJA3* expression than control cells (Supplemental Figure S5B, http://links.lww.com/HEP/I72). Furthermore, a luciferase reporter assay, controlled by the *DNAJA3* promoter and encompassing rs3747579, demonstrated elevated luciferase activity for the rs3747579-CC allele relative to its rs3747579-TT counterpart (Supplemental Figure S5C, http://links.lww.com/HEP/I72).

Next, we conducted a functional study to explore the role of *DNAJA3* in NASH-HCC. We performed a gene-based phenome-wide association studies and found a strong association between *DNAJA3* and serum lipids, including triglyceride and hepatic damage marker alkaline phosphatase (Supplemental Figure S6A, http://links.lww.com/HEP/I72). In addition, we found that the expression of *DNAJA3* was significantly associated with fatty liver disease (Supplemental Figure S6B, http://links.lww.com/HEP/I72). Knockdown *DNAJA3* led to a marked increase in lipid droplet accumulation compared to control cells, whereas CORO7 knockdown did not produce such an effect. However, neither knockdown resulted in cell death (Supplemental Figure S6C–F, http://links.lww.com/HEP/I72). *DNAJA3* expression was significantly decreased in NASH compared to normal (Supplemental Figure S7A, http://links.lww.com/HEP/I73), and in NASH-HCC compared to non-NASH-HCC (Supplemental Figure S7B, C, http://links.lww.com/HEP/I73). Furthermore, *DNAJA3* expression was significantly decreased in HCC compared to the adjacent nontumor liver tissues in all examined cohorts (Figure S7D–G, http://links.lww.com/HEP/I73). In addition, *DNAJA3* expression was significantly reduced in cirrhotic livers compared to noncirrhotic livers (Supplemental Figure S7H, I, http://links.lww.com/HEP/I73). Consistent with the risk allele data, *DNAJA3* expression in HCC was significantly associated with overall survival (Supplemental Figure S7J, K, http://links.lww.com/HEP/I73). Taken together, rs3747579-TT may act as a disease allele associated with a reduced *DNAJA3* expression linked to NASH and NASH-related HCC.

Dnaja3-deficient mice develop NAFLD, NASH, and HCC

To validate the function of *Dnaja3*, mice with a conditional knockout of *Dnaja3* in hepatocytes (*Dnaja3*$^{+/-}$ and *Dnaja3*$^{-/-}$) were constructed to examine the influence of reduced gene expression on the progression of NASH to HCC (Figure 2A, B). The details for liver conditional knockout mice of *Dnaja3* generation are available in Supplemental Methods, http://links.lww.com/HEP/I70 and Supplemental Figure S8, http://links.lww.com/HEP/I73. In brief, a genetically modified mouse line with exons 1 and 2 of *Dnaja3* flanked by *loxP* elements (*Dnaja3*$^{f/f}$) was generated and crossed with albumin-Cre to generate the *Dnaja3* mice (Figure 2A). PCR genotyping, mRNA expression, and protein levels analyses revealed an efficient depletion of *Dnaja3* in hepatocytes of *Dnaja3*$^{-/-}$ mice (Supplemental Figures S9A, http://links.lww.com/HEP/I73, Figure 2C, and S9B, http://links.lww.com/HEP/I73). Interestingly, we observed that *Dnaja3*$^{-/-}$ mice were undergoing retarded growth during the first 12 months under normal diet, especially in the first month (Supplemental Figure S9C, D, http://links.lww.com/HEP/I73). The *Dnaja3*$^{-/-}$ mice showed elevated serum levels of aspartate aminotransferase and alanine aminotransferase (Supplemental Figure S9E, http://links.lww.com/HEP/I73 and Figure 2D). We found evidence of fatty liver in 1-month-old *Dnaja3*$^{-/-}$ mice and NASH in 13 months old *Dnaja3*$^{-/-}$ mice under normal diet (Figure 2E–H and Supplemental Figure S9F, http://links.lww.com/HEP/I73), with a similar tendency of the body weight change (Supplemental Figure S9D, http://links.lww.com/HEP/I73). In evaluating the commonly used NASH activity score (a composite score of steatosis, hepatocellular ballooning, and lobular inflammation) for histological staging and grading system of human NASH, we found an elevated NASH score increases 6-fold in the liver of *Dnaja3*$^{-/-}$ mice compared to heterozygous or *Dnaja3*$^{f/f}$ mice ($p < 0.005$) (Figure 2G). In addition, the serum cholesterol levels were elevated in *Dnaja3*$^{-/-}$ mice (Figure 2I).

Histologically confirmed the male *Dnaja3*$^{-/-}$ mice developed hepatocellular nodules at the age of 11 months under normal diet (Figures 2J, 2K and Supplemental Figure S9G, http://links.lww.com/HEP/I73). Furthermore, 100% of the *Dnaja3*$^{-/-}$ and heterozygous male mice spontaneously developed liver tumors by 13 and 21 months, respectively (Figure 2J, K). In addition, Ki67-positive cells in the liver were elevated in *Dnaja3*$^{-/-}$ mice as a cell growth marker (Supplemental Figure S9H, http://links.lww.com/HEP/I73). By 21 months, some of the knockout mice also developed lung tumor lesions (Supplemental Figure S9I, http://links.lww.com/HEP/I73). These results indicate that hepatic *Dnaja3* deficiency may be associated with the NASH phenotype and tumorigenesis.

Dnaja3-deficient mice sequentially developed a fatty liver, NASH, advanced fibrosis, and HCC and enhanced by diethylnitrosamine

To create DNA damage-induced metabolic changes resembling human NASH-HCC, we subjected Dnaja3-deficient mice to diethylnitrosamine (DEN), a known carcinogen that triggers DNA damage, inflammation, and hepatocarcinogenesis.[26] We found that DEN accelerated HCC development in *Dnaja3*-deficient male mice, with a significantly shorter time compared to heterozygous or *Dnaja3*$^{-/-}$ mice without DEN (p <0.0001) (Figures 2J, K and 3A–C). Hepatocellular nodules could be observed in the 3-month DEN-treated *Dnaja3*$^{-/-}$ mice (Figure 3A–C). Histological examination with hematoxylin-eosin staining showed that these macroscopic tumors represented early-stage to advanced HCC (Figure 3B). At 6 months, the DEN-treated *Dnaja3*$^{-/-}$ mice exhibited more tumors and larger tumor size than DEN-treated *Dnaja3*$^{+/-}$ or *Dnaja3*$^{f/f}$ mice (Figure 3A–C). Similar results could be found in female mice (Supplemental Figure S10, http://links.lww.com/HEP/I73). However, a sex disparity was observed in our transgenic mouse models with or without DEN treatment, where the earlier onset of HCC

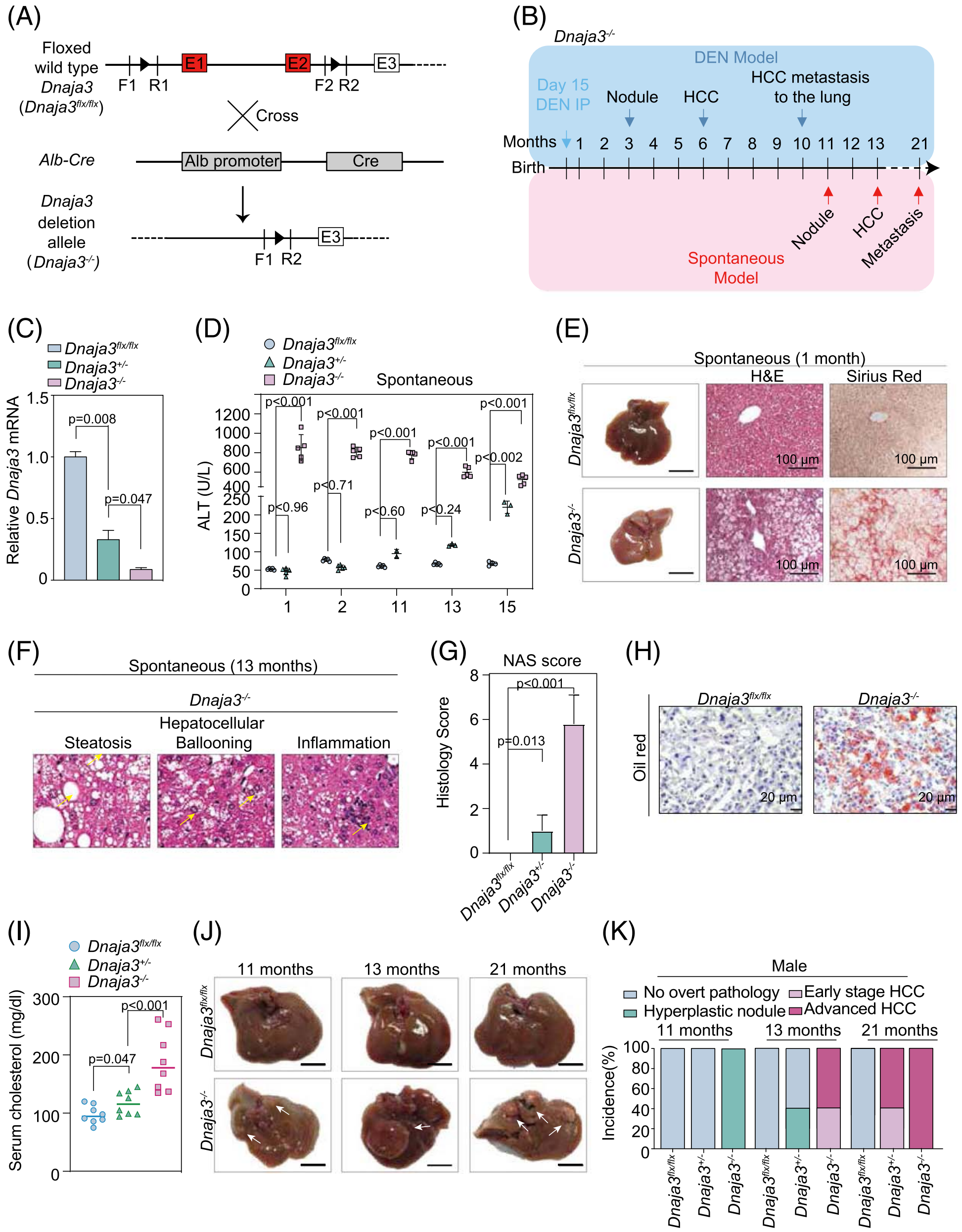

FIGURE 2 Mice with hepatocyte-specific *Dnaja3* depletion developed NASH-dependent HCC spontaneously. (A) Generation of mice with *Dnaja3* deletion in hepatocytes. Two *loxP* (locus of X-over P1) sites were inserted (black arrowhead) at exons 1 and 2 of the *Dnaja3* gene as the targeted locus (red solid boxes). Cross-breeding of *Dnaja3*$^{f/f}$ mice with albumin-Cre mice led to hepatic *Dnaja3* deficiency. The details of the generation of *Dnaja3*$^{flx/flx}$ mice on a C57BL/6N background were available in Supplemental Methods, http://links.lww.com/HEP/I70. (B) Pathological progression of male *Dnaja3*$^{-/-}$ mice for DEN-induced and spontaneous mouse models. (C) mRNA levels of *Dnaja3* in liver tissues from *Dnaja3*$^{f/f}$, *Dnaja3*$^{+/-}$, and *Dnaja3*$^{-/-}$ mice (n = 5). (D) Enzymatic activity of ALT was monitored in serum of spontaneous male *Dnaja3*$^{f/f}$, *Dnaja3*$^{+/-}$, and *Dnaja3*$^{-/-}$ mice (n = 5). (E) Representative gross liver images from 1-month-old spontaneous *Dnaja3*$^{f/f}$ and *Dnaja3*$^{-/-}$ male mice (left panel). Images of H&E staining of representative liver sections obtained from 1-month-old male mice (middle panel). Sirius Red staining of liver sections from 1-month spontaneous *Dnaja3*$^{f/f}$ and *Dnaja3*$^{-/-}$ mice (right panel). (F) H&E staining of liver sections from 13-month spontaneous male mice depicting the individual component of steatohepatitis: Steatosis, Hepatocyte Ballooning and Inflammation as indicated by the yellow arrow. (G) Steatosis, Hepatocyte Ballooning, and Inflammation scores were quantified from 2F. Results were expressed as mean ± SD. (H) Representative images of Oil Red O staining of liver sections from 13-month spontaneous male *Dnaja3*$^{f/f}$ and *Dnaja3*$^{-/-}$ mice. (I) Serum level analysis of cholesterol was monitored at 13-month spontaneous male mice (*Dnaja3*$^{f/f}$ and *Dnaja3*$^{-/-}$: n = 7; *Dnaja3*$^{+/-}$: n = 8). (J) Representative gross liver images from 11-, 13-, and 21-month-old spontaneous *Dnaja3*$^{f/f}$, *Dnaja3*$^{+/-}$ and *Dnaja3*$^{-/-}$ male mice. (K) Summary of the incidence of *Dnaja3*-mediated hyperplastic nodules, HCC (advanced and early stage), and the presence of no over pathological lesions in the livers from 11-, 13-, and 21-month-old spontaneous male mice (n = 5). Abbreviations: ALT, alanine aminotransferase; DEN, diethylnitrosamine; *Dnaja3*, DnaJ Heat Shock Protein Family (Hsp40) Member A3; H&E, hematoxylin-eosin; NAS, NASH activity score.

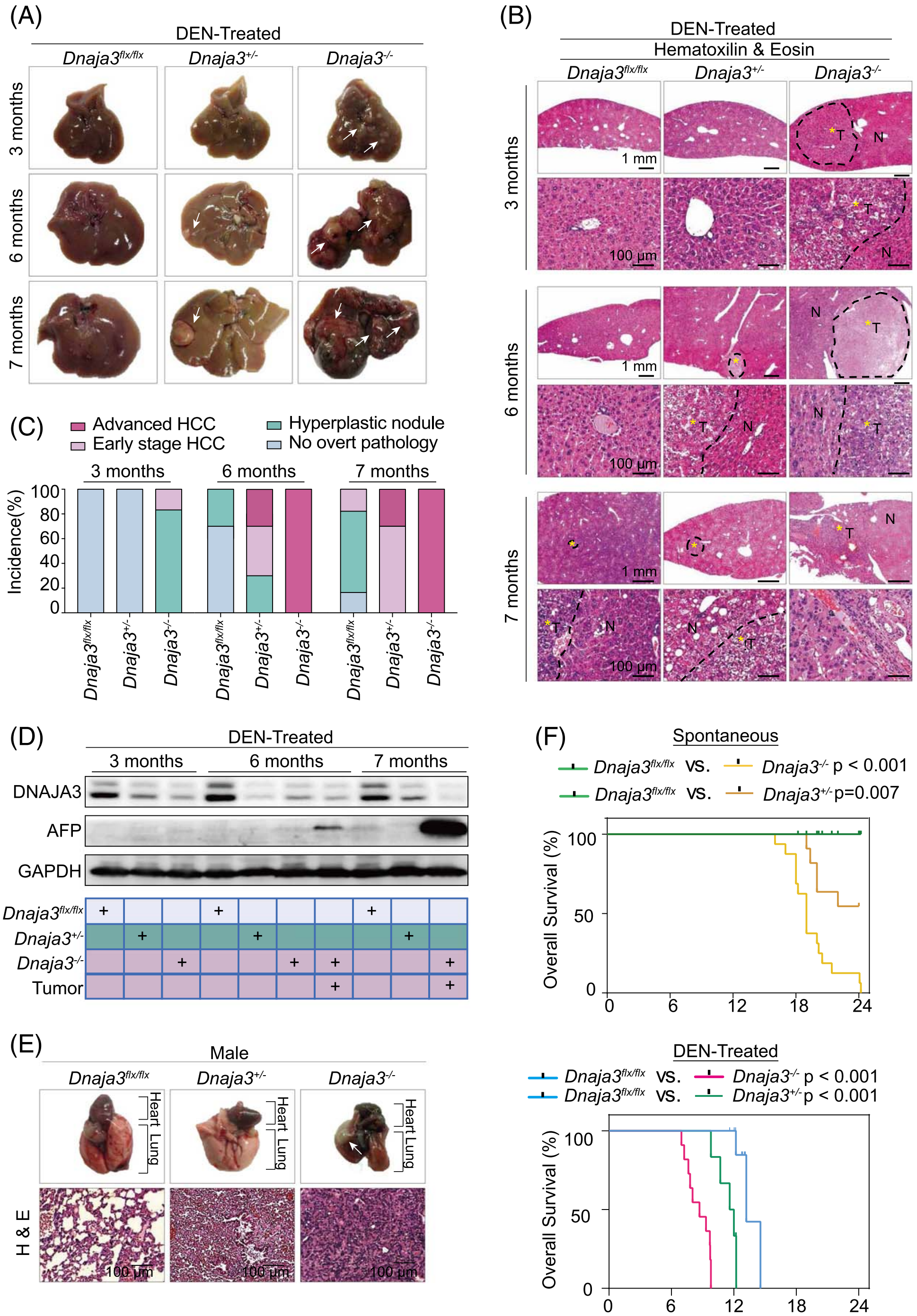

FIGURE 3 Hepatic *Dnaja3* deficiency promotes DEN-induced HCC. (A) Gross liver images from DEN-treated male *Dnaja3*$^{f/f}$, *Dnaja3*$^{+/-}$, and *Dnaja3*$^{-/-}$ mice. (B) H&E staining of liver sections from DEN-treated male *Dnaja3*$^{f/f}$, *Dnaja3*$^{+/-}$, and *Dnaja3*$^{-/-}$ mice. Yellow star indicating the tumors. (C) Summary of hyperplastic nodules, HCC (advanced and early stage), and no overt pathological lesions in the livers from DEN-treated male mice (n = 5). (D) Immunoblots showing DNAJA3, AFP, and GAPDH protein levels in the livers of DEN-treated mice. (E) Representative gross lung images from 10-month-old DEN-treated *Dnaja3*$^{f/f}$, *Dnaja3*$^{+/-}$, and *Dnaja3*$^{-/-}$ male mice (upper panel). Images of H&E staining of representative lung sections obtained from 10-month-old DEN-treated *Dnaja3*$^{f/f}$, *DNAJA3*$^{+/-}$, and *Dnaja3*$^{-/-}$ male mice (lower panel). (F) Kaplan-Meier analyses showing the overall survival of spontaneous (upper panel) or DEN-treated (lower panel) *Dnaja3*$^{f/f}$, and *Dnaja3*$^{-/-}$ male mice (DEN-treated group: *Dnaja3*$^{f/f}$: n = 20; *Dnaja3*$^{-/-}$: n = 11; *DNAJA3*$^{+/-}$: n = 6; spontaneous group: *Dnaja3*$^{f/f}$ and *Dnaja3*$^{-/-}$: n = 16; *DNAJA3*$^{+/-}$: n = 11). Abbreviations: AFP, alpha-fetoprotein; DEN, diethylnitrosamine; *Dnaja3*, DnaJ Heat Shock Protein Family (Hsp40) Member A3; H&E, hematoxylin-eosin; GAPDH, glyceraldehyde 3-phosphate dehydrogenase; N, normal area; T, tumor area.

occurred in male mice than in the female mice (Figures 2J, K, 3A–C and Supplemental Figure S10, http://links.lww.com/HEP/I73). Induction of NASH-HCC was accompanied by elevated levels of an HCC marker alpha-fetoprotein in DEN-treated *Dnaja3*$^{-/-}$ mice (Figure 3D). Moreover, 40% of the DEN-treated

Dnaja3$^{-/-}$ mice developed lung metastasis, while no metastatic tumor was found in the DEN-treated *Dnaja3*$^{f/f}$ mice (Figure 3E). Furthermore, the overall survival of *Dnaja3*$^{-/-}$ mice was significantly worse than that of the heterozygous or *Dnaja3*$^{f/f}$ mice both without and with DEN treatment (Figure 3F). Notably, DEN-treated *Dnaja3*$^{-/-}$ mice had a 60% decrease in median survival compared to the untreated *Dnaja3*$^{-/-}$ mice (Figure 3F).

Grossly and histologically, the liver of DEN-treated *Dnaja3*$^{-/-}$ mice displayed many typical characteristics of human NASH (Figure 4 and Supplemental Figure S11, http://links.lww.com/HEP/I73). Within a month, these mice exhibited noticeable liver enlargement and discoloration, indicating early lipid accumulation (Supplemental Figure S11A, http://links.lww.com/HEP/I73). Electron microscopy confirmed lipid droplet buildup in the liver after 1 month of DEN treatment (Supplemental Figure S11B, http://links.lww.com/HEP/I73). Histological analysis confirmed the presence of extensive microvesicular steatosis by 1 month and large droplet steatosis by 6 months (Figure 4A). By 3 months, the DEN-treated *Dnaja3*$^{-/-}$ mice expressed significantly higher levels of proinflammatory cytokines and chemokines (Supplemental Figure S11C, http://links.lww.com/HEP/I73), along with the presence of lymphocytic infiltrates and ectopic lymphoid-like structures (Figure 4B), the typical features of NASH.[27] An increase of F4/80-positive macrophage infiltrates (KCs) was evident in the liver of both 3- and 6-month-old *Dnaja3*$^{-/-}$ mice (Supplemental Figure S11D, http://links.lww.com/HEP/I73). However, these features were absent in the DEN-treated *Dnaja3*$^{f/f}$ mice during the same period.

The liver of DEN-treated *Dnaja3*$^{-/-}$ mice showed a marked increase in apoptosis compared to their *Dnaja3*$^{f/f}$ counterparts, as evidenced by terminal deoxynucleotidyl transferase dUTP nick end labeling assay results (Supplemental Figure S11E, http://links.lww.com/HEP/I73) and further validated by immunoblot analyses of cleaved caspase-3 (Supplemental Figure S11F, http://links.lww.com/HEP/I73). Liver damage was more pronounced in the 6-month DEN-treated *Dnaja3*$^{-/-}$ mice, accompanied by elevated serum levels of aspartate aminotransferase and alanine aminotransferase (Figure 4C). Moreover, markers of oxidative stress *Nfe2l2*[28] and *Grp78*[29] were significantly increased in the liver of DEN-treated *Dnaja3*$^{-/-}$ mice (Supplemental Figure S11G, http://links.lww.com/HEP/I73). The proliferation marker Ki67 and collagen deposition (Sirius red staining) were also elevated in the liver of 6-month DEN-treated Dnaja3-/- mice (Supplemental Figures S11H, http://links.lww.com/HEP/I73 and Figure 4D). Consistently, the NASH activity score values were significantly elevated 7-fold in the liver of 6-month DEN-treated *Dnaja3*$^{-/-}$ mice ($p < 0.005$) (Figure 4E–G). Taken together, these results indicate that hepatic *Dnaja3* deficiency along with DEN-induced liver damage may accelerate NASH development.

Dnaja3 deficiency contributes to mitochondrial dysfunction and excessive fat accumulation

To determine molecular alterations of hepatic *Dnaja3* deficiency, we analyzed transcriptome profiles of the livers from 1-, 3-, or 6-month-old DEN-treated *Dnaja3*$^{-/-}$ and *Dnaja3*$^{f/f}$ mice. Among the top-20 downregulated pathways in the DEN-treated *Dnaja3*$^{-/-}$ livers, many were related to the mitochondrial function, such as mitochondrial translation, oxidative phosphorylation (OXPHOS), and fatty acid oxidation (FAO) pathways (Figure 5A; left panel), and these features persisted over time (Figure 5A; right panel). In contrast, the top-upregulated pathways in the livers of DEN-treated *Dnaja3*$^{-/-}$ mice were related to immune cell infiltration and collagen organization (Figure 5A). Furthermore, the altered pathways in the liver of DEN-treated *Dnaja3*$^{-/-}$ mice could also be found in patients with NAFLD, NASH, cirrhosis, and HCC (Supplemental Figure S12A, http://links.lww.com/HEP/I74). Several of the most affected genes in *Dnaja3*$^{-/-}$ livers, including *LGALS3*, *SPP1*, and *IGFBP1*,[30] are also linked to human NASH (Supplemental Figure S12B, http://links.lww.com/HEP/I74). We found a significant concordance of the *Dnaja3*$^{-/-}$ mice gene expression patterns at 3 or 6 months to the human NASH transcriptome (false discovery rate 0.02 and 0.11, respectively) (Figure 5B, C). Moreover, by 6 months, every *Dnaja3*$^{-/-}$ mouse had developed HCC, and the gene expression from these mice strongly correlated with human HCC data (Supplemental Figure S12C–E, http://links.lww.com/HEP/I74). In addition, the pattern of gene expression within the transcriptome from *Dnaja3*$^{-/-}$ mice at 3 or 6 months demonstrated strong concordance with human cirrhosis (Fisher p-value: 0.04 and 0.04, respectively) (Supplemental Figure S12D, E, http://links.lww.com/HEP/I74).

Given *DNAJA3*'s role as a mitochondrial chaperone, we used electron microscopy to study hepatocyte mitochondrial morphology. In spontaneous *Dnaja3*$^{-/-}$ mice, hepatocytes exhibited swollen, round, and hypodense mitochondria, unlike their *Dnaja3*$^{f/f}$ counterparts (Supplemental Figure S13, http://links.lww.com/HEP/I74). By the first month of DEN treatment in *Dnaja3*$^{-/-}$ mice, pronounced mitochondrial swelling was evident, characterized by complete cristae loss and cytoplasmic material intrusion (Figure 5D). By the third month, several mitochondria appeared diminutive, showcasing either rudimentary cristae or significant proteolysis (Figure 5D). In contrast, DEN-treated *Dnaja3*$^{f/f}$ livers showed mitochondria with intact membranes and preserved cristae structure (Figure 5D). Subsequent assays revealed elevated mRNA levels of lipid droplet proteins *Plin2* and *Plin3* (Figure 5E). This was synchronized with heightened serum cholesterol and decreased triglycerides (Figure 5F, G). These findings suggest that

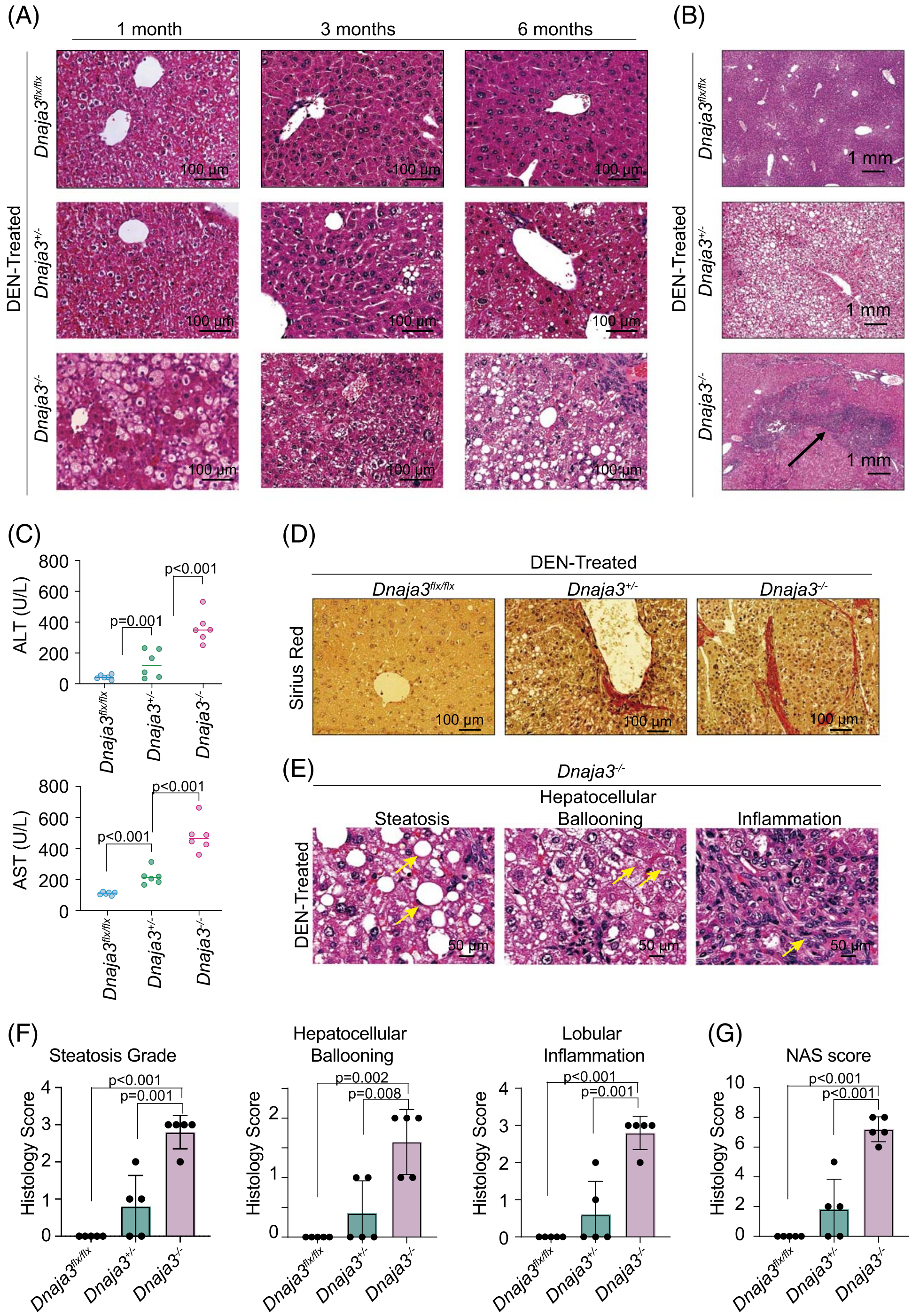

FIGURE 4 The histopathology of *Dnaja3* deletion mice associated with the development of NAFLD and NASH phenotype. (A) Hematoxylin-eosin staining of liver sections from DEN-treated *Dnaja3*$^{f/f}$, *Dnaja3*$^{+/-}$, and *Dnaja3*$^{-/-}$ male mice. (B) Hematoxylin-eosin staining of liver sections from 6-month DEN-treated *Dnaja3*$^{f/f}$, *Dnaja3*$^{+/-}$, and *Dnaja3*$^{-/-}$ male mice. Black arrow indicates lymphocytic infiltrate-like structures. (C) Enzymatic activity of ALT and AST was monitored in serum of 6-month DEN-treated and spontaneous *Dnaja3*$^{f/f}$, *Dnaja3*$^{+/-}$, and *Dnaja3*$^{-/-}$ male mice (n = 6). (D) Sirius Red staining of liver sections from 6-month DEN-treated *Dnaja3*$^{f/f}$, *Dnaja3*$^{+/-}$, and *Dnaja3*$^{-/-}$ male mice. (E) Hematoxylin-eosin staining of liver sections from 6-month DEN-treated male mice depicting the individual component of steatohepatitis: Steatosis, Hepatocyte Ballooning, and Inflammation as indicated by the yellow arrow. (F) The histological score for Steatosis, Hepatocyte Ballooning, and Inflammation. The score was quantified from 6-month DEN-treated male mice. Results were expressed as mean ± SD. (G) The histological score for NASH activity. NAS scores were quantified from 6-month DEN-treated male mice. Results were expressed as mean ± SD. Abbreviations: ALT, alanine aminotransferase; AST, aspartate aminotransferase; DEN, diethylnitrosamine; *Dnaja3*, DnaJ Heat Shock Protein Family (Hsp40) Member A3; NAS, NASH activity score.

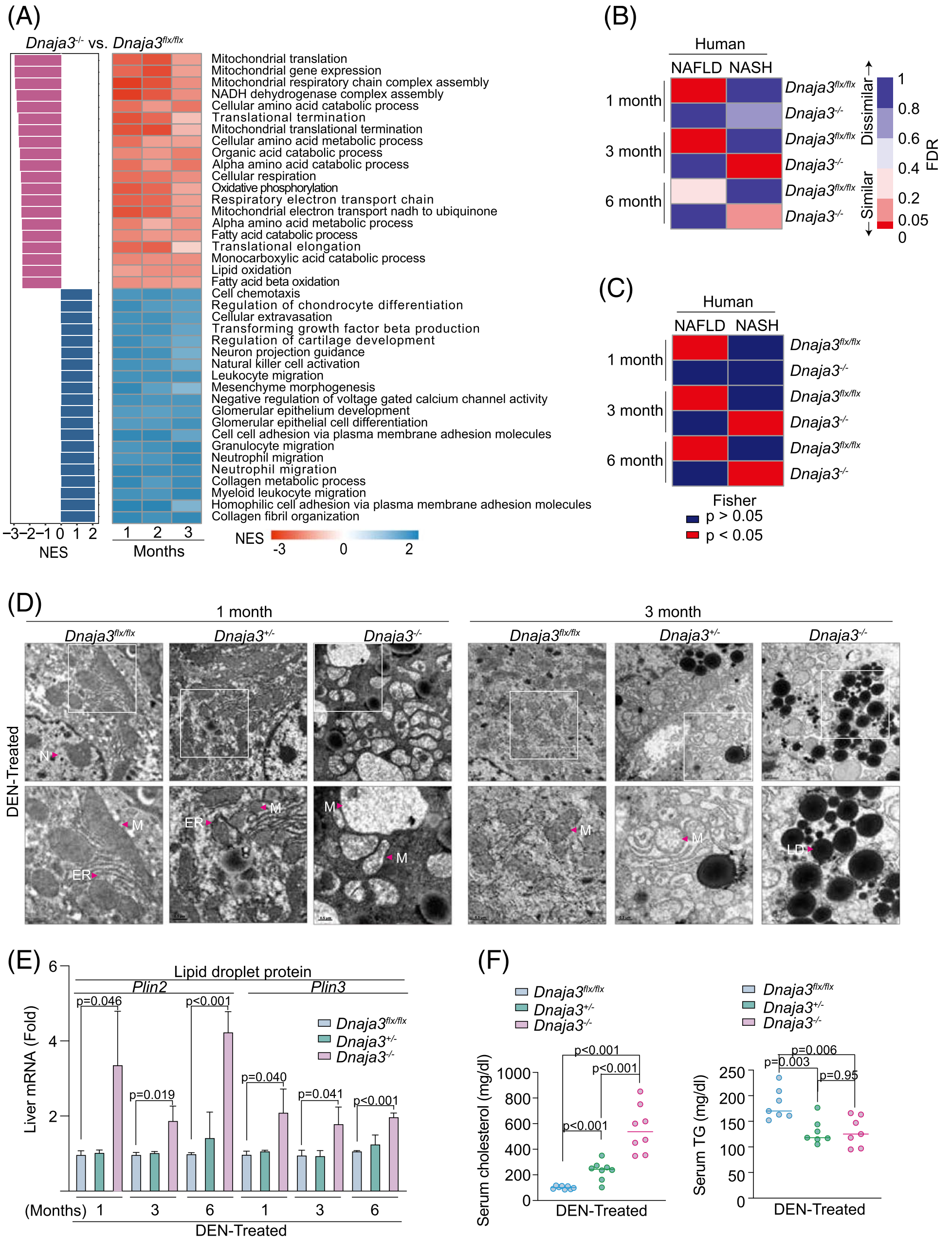

FIGURE 5 Hepatic *Dnaja3* deficiency causes dysregulated mitochondrial and fatty acid metabolism. (A) Bar plots showing the most significant gene sets enriched in the livers from DEN-treated *Dnaja3*$^{-/-}$ versus *Dnaja3*$^{f/f}$ mice by gene set enrichment analysis. NES indicates the normalized enrichment score in the gene set enrichment analysis algorithm (left panel). Heatmap showing NES of 40 gene sets (rows) across clustering. Each pathway is significantly upregulated or downregulated in the liver tissue from *Dnaja3*$^{-/-}$ mice versus *Dnaja3*$^{f/f}$ male mice for 1, 3, and 6 months (right panel). (B) Similarity between global transcriptome of livers from DEN-treated *Dnaja3*$^{-/-}$ or *Dnaja3*$^{f/f}$ mice for 1, 3, 6 months and global transcriptome in liver biopsy tissues from 7 human patients with NASH and 26 individuals with NAFLD in siliac acid cohort using subclass mapping algorithm. FDR values are represented as colors in a heatmap. (C) Similarity between global transcriptome of livers from DEN-treated *Dnaja3*$^{-/-}$ or *Dnaja3*$^{f/f}$ mice for 1, 3, and 6 months and global transcriptome in liver biopsy tissues from 7 human patients with NASH and 26 individuals with NAFLD in SA cohort using subclass mapping algorithm. A heatmap showing *p*-values from the Fisher test. (D) Transmission electron micrographs analyses of liver samples from DEN-treated *Dnaja3*$^{f/f}$ and *Dnaja3*$^{-/-}$ mice. (E) mRNA levels of lipid droplet protein in the livers of male mice. Results were expressed as mean ± SD. (F-G) Serum level analysis of cholesterol (E) and TG (F) were monitored at 6-month DEN-treated male mice (n = 7). Abbreviations: DEN, diethylnitrosamine; *Dnaja3*, DnaJ Heat Shock Protein Family (Hsp40) Member A3; ER, endoplasmic reticulum; FDR, false discovery rate; LD, lipid droplets; M, mitochondria; N, nuclei; NES, normalized enrichment score; TG, triglyceride.

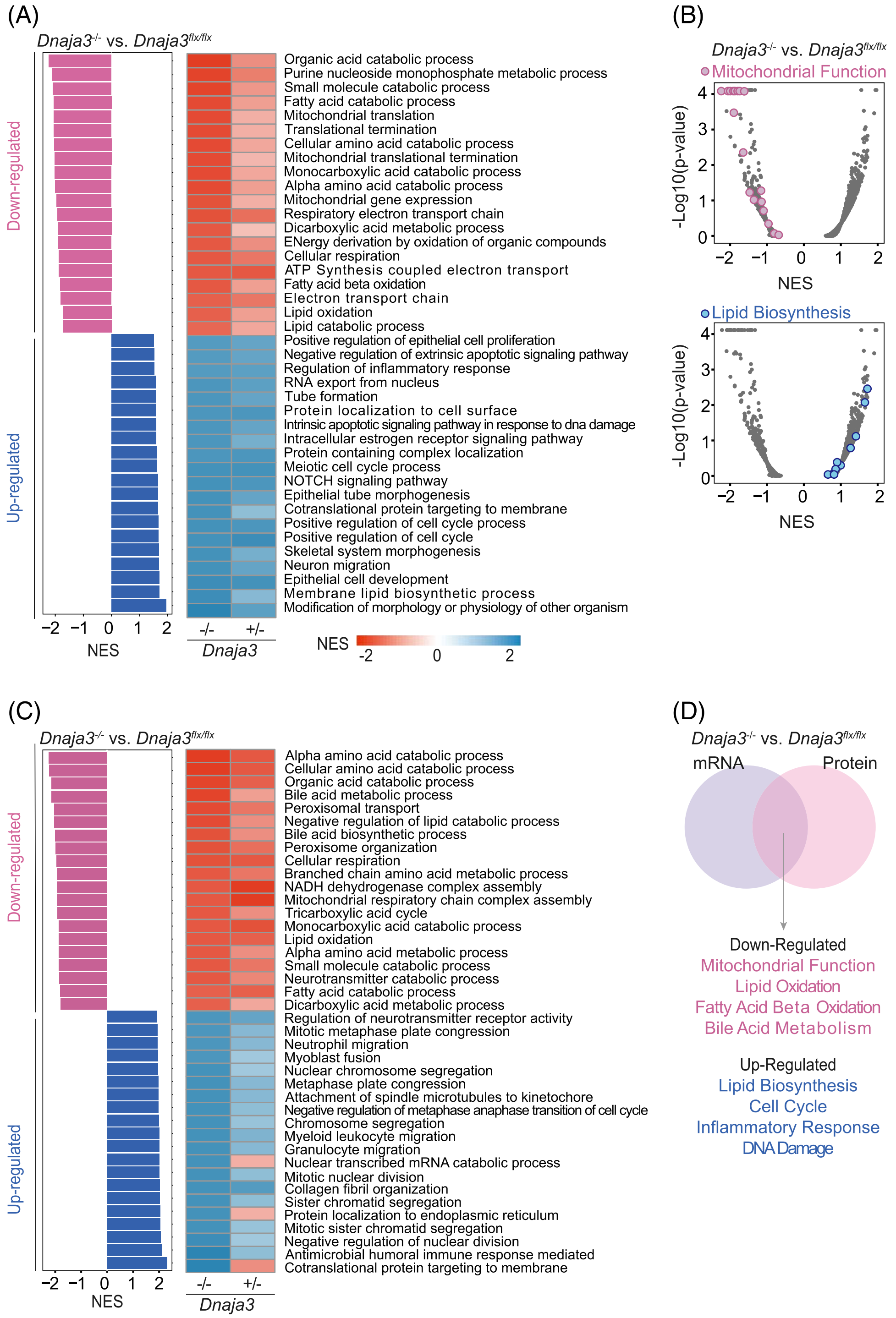

FIGURE 6 Tumor development is associated with mitochondrial dysfunction and fatty acid metabolic dysregulation in DEN-treated *Dnaja3*$^{-/-}$ mice.(A) Bar plots showing the most significant gene set enriched in protein levels of livers from DEN-treated *Dnaja3*$^{-/-}$ versus *Dnaja3*$^{f/f}$ mice by GSEA (left panel). Each pathway is significantly upregulated or downregulated in the *Dnaja3*$^{+/-}$ or *Dnaja3*$^{-/-}$ mice versus *Dnaja3*$^{f/f}$ male mice for 6 months (right panel). (B) Volcano plots showing gene sets enriched in the protein levels of liver tissue from DEN-treated *Dnaja3*$^{-/-}$ male mice versus *Dnaja3*$^{f/f}$ (gray dots; Welch *t* test). Selected enriched mitochondrial function (upper panel) and lipid biosynthesis (lower panel) pathways are colored. (C) Bar plots showing the most significant gene set enriched in mRNA levels of livers from DEN-treated *Dnaja3*$^{-/-}$ versus *Dnaja3*$^{f/f}$ male mice by GSEA (left panel). Each pathway is significantly upregulated or downregulated in the *Dnaja3*$^{+/-}$ or *Dnaja3*$^{-/-}$ mice versus *Dnaja3*$^{f/f}$ male mice for 6 months (right panel). (D) Venn diagram depicting the overlapping pathways between the RNA-Seq and proteomic analysis with significantly altered functional categories in liver tissue from *Dnaja3*$^{-/-}$ male mice versus *Dnaja3*$^{f/f}$ male mice. Abbreviations: *Dnaja3*, DnaJ Heat Shock Protein Family (Hsp40) Member A3; NES, normalized enrichment score.

Dnaja3 deficiency could precipitate mitochondrial aberrations, further intensifying hepatocyte steatosis.

Dnaja3 deficiency developed HCC links to mitochondrial bile acid production and fatty acid oxidation

To gain insights into proteomic changes during NASH to HCC progression, we performed an liquid chromatography-tandem mass spectrometry–based proteomic analysis with livers collected from 6-month DEN-treated mice. Differentially altered proteins were subjected to pathway analysis. We found that many mitochondrial-related pathways, including mitochondrial FAO, amino acid catabolism, and mitochondrial translation, were enriched, while lipid biosynthesis and cell cycle proteins were significantly upregulated in liver tumors of DEN-treated *Dnaja3*$^{-/-}$ mice (Figure 6A). There was a significant enrichment in the lipid biosynthesis pathways but a significant depletion of pathways related to mitochondrial functions in tumors from DEN-treated *Dnaja3*$^{-/-}$ mice (Figure 6B). We found a good concordance of affected pathways between transcriptomic and proteomic analyses (Figure 6C, D).

We then searched *DNAJA3*-interacting proteins using 3 protein-protein interaction network databases and found 17 mitochondrial proteins potentially binding to *DNAJA3*, and these proteins could be grouped as 4 clusters by Markov Clustering (Supplemental Figure S14A, http://links.lww.com/HEP/I74). Interestingly, we found that many *DNAJA3*-interacting mitochondrial proteins were reduced in the liver of DEN-treated *Dnaja3*$^{-/-}$ mice (Supplemental Figure S14B, http://links.lww.com/HEP/I74). Pathway enrichment analysis revealed NAFLD as the top significant hit among the *DNAJA3*-interacting client proteins (Supplemental Figure S14C, http://links.lww.com/HEP/I74). Consistently, pathway analysis of *DNAJA3*-interacting proteins revealed enrichment of biological processes related to mitochondrion functions (Supplemental Figure S14D, http://links.lww.com/HEP/I74).

We next mapped our proteomic data to known human metabolic networks and found that the mitochondrial protein levels were highly downregulated in the liver of DEN-treated *Dnaja3*$^{-/-}$, which was linked to several metabolic pathways, such as OXPHOS, FAO, and bile acid biosynthesis (Figure 7A). In parallel, protein levels in fatty acid and cholesterol biosynthetic pathways as well as cytosolic proteins involved in glycolysis, the pentose phosphate pathway, and the serine/glycine biosynthetic pathway were highly upregulated in the liver of DEN-treated *Dnaja3*$^{-/-}$ mice (Figure 7A). We validated the expression of the key genes using reverse transcription-polymerase chain reaction analyses (Figure 7B, C). We also performed metabolomic profiling and found that consistent with proteomic data described above, both bile acids and the FAO end-products (Acetyl-CoA) were significantly decreased, while the amount of saturated and monounsaturated fatty acids as well as pyruvate and lactate (products of glycolysis) and 6PG (a key intermediate in the pentose phosphate pathway) were significantly increased in the livers of DEN-treated *Dnaja3*$^{-/-}$ mice (Figure 7A and Supplemental Table S16, http://links.lww.com/HEP/I71 and S17, http://links.lww.com/HEP/I71).

To further explore mitochondrial functions linked to *DNAJA3* deficiency–induced malignant transformation of hepatocytes, we analyzed HCC cells isolated from DEN-treated *Dnaja3*$^{-/-}$ and *Dnaja3*$^{f/f}$ mice. We found a reduced expression of mitochondrial OXPHOS subunits belonging to complexes I, III, and V in *Dnaja3*$^{-/-}$ tumor cells compared to those of *Dnaja3*$^{f/f}$ (Supplemental Figure S15A, http://links.lww.com/HEP/I74). We also characterized the level of MitoSOX fluorescence in the *Dnaja3*$^{-/-}$ cells, which serves as an indicator of mitochondrial reactive oxygen species levels by flow cytometry and found that *Dnaja3*$^{-/-}$ tumors displayed markedly increased mitochondrial reactive oxygen species levels (Supplemental Figure S15B, http://links.lww.com/HEP/I74). Moreover, the basal oxygen consumption rate was significantly decreased while the extracellular acidification rate was significantly increased in the *Dnaja3*$^{-/-}$ tumors (Supplemental Figure S15C, http://links.lww.com/HEP/I74). In addition, the ATP levels and ATP/ADP ratio were significantly reduced in *Dnaja3*$^{-/-}$ tumors (Supplemental Figure S15D, http://links.lww.com/HEP/I74). We also assessed mitochondrial membrane potential ($\Delta\Psi M$) using JC-1 fluorescence to evaluate the mitochondria polarization state, with lower $\Delta\Psi M$ being indicated by the shift to green fluorescence from red fluorescence. We found that the JC-1 green fluorescence was markedly increased in *Dnaja3*$^{-/-}$ tumors versus *Dnaja3*$^{f/f}$ tumors (Supplemental Figure S15E, http://links.lww.com/HEP/I74). Taken together, our results are consistent with the hypothesis that *Dnaja3* deficiency may induce hepatic mitochondrial dysfunctions, which in turn induce HCC.

To clarify Dnaja3's role against mitochondrial dysfunction and lipid accumulation, we conducted a rescue experiment with *Dnaja3*$^{-/-}$ mice. These mice were transduced with an adeno-associated virus (AAV) overexpressing *Dnaja3* (pssAAV-CB-*Dnaja3*) or a control vector (pssAAV-CB-Control). Within 14 days, effective *Dnaja3* overexpression was noted in *Dnaja3*$^{-/-}$ mice livers, as indicated in Supplemental Figure S16A, http://links.lww.com/HEP/I74, B, http://links.lww.com/HEP/I74. After 12 weeks, pssAAV-CB-driven *Dnaja3* significantly countered the effects of *Dnaja3* deficiency on mitochondrial genes ATP5A and NDUFB8 while inhibiting mitochondrial FAO gene ACACB (Supplemental Figure S16C, http://links.lww.com/HEP/I74). Notably, the AAV-treated groups exhibited a significant

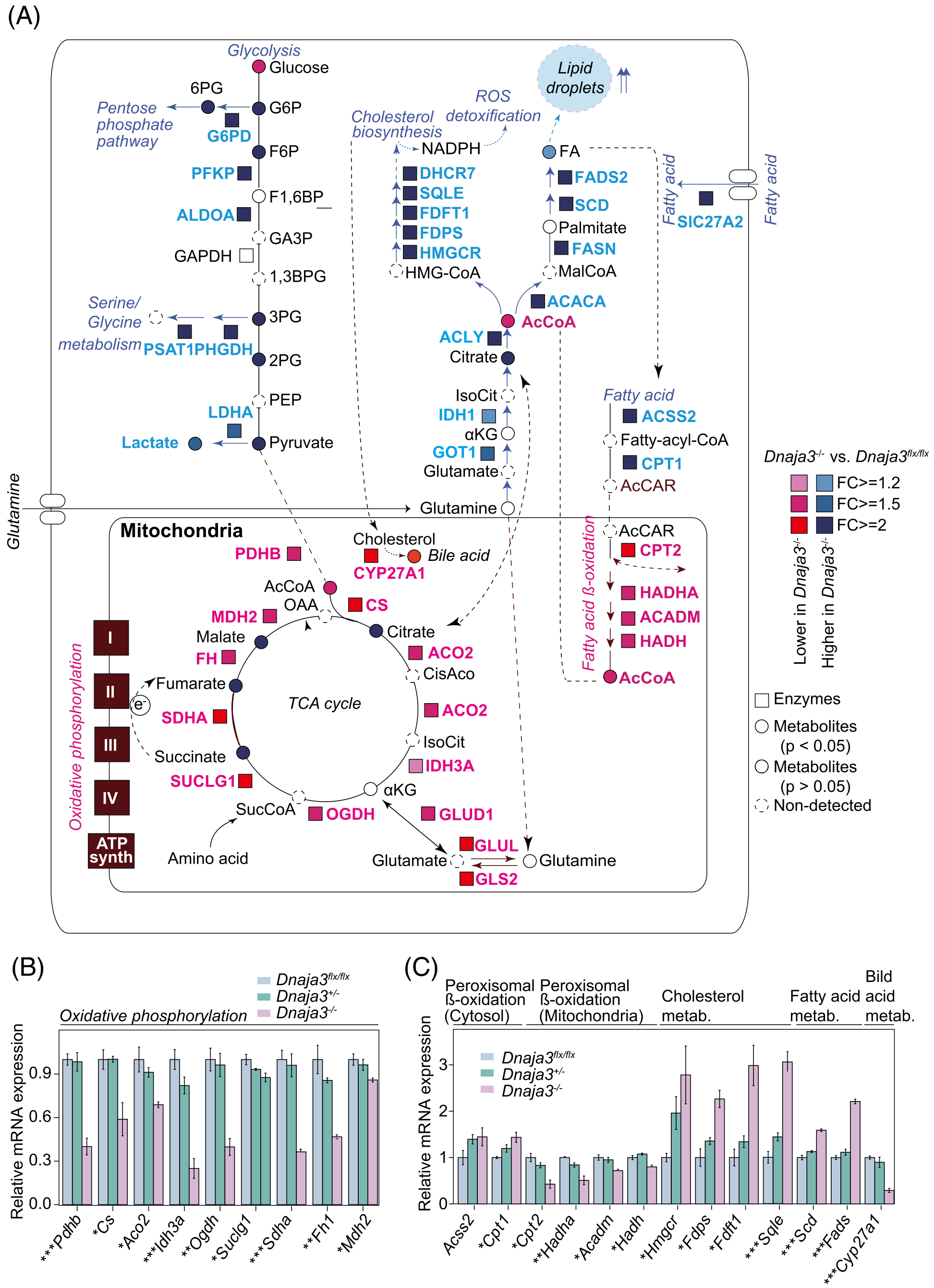

FIGURE 7 *Dnaja3* deletion induces lipid accumulation and cholesterol synthesis through blocking mitochondrial function. (A) A diagram describing the changes in different metabolic pathways in livers from *Dnaja3*$^{-/-}$ mice compared to *Dnaja3*$^{f/f}$ male mice. Red square and blue square symbols represent downregulated and upregulated, respectively, metabolic enzymes in livers from *Dnaja3*$^{-/-}$ mice versus *Dnaja3*$^{f/f}$ mice. Red round and blue round symbols represent downregulated and upregulated metabolites in livers from *Dnaja3*$^{-/-}$ mice versus *Dnaja3*$^{f/f}$ male mice. (B and C) Differential expression of OXPHOS (B) and fatty acid metabolic (C) enzymes in livers from 6-month DEN-treated *Dnaja3*$^{f/f}$, *Dnaja3*$^{+/-}$, and *Dnaja3*$^{-/-}$ male mice. Results were expressed as mean ± SD. *$p<0.05$; **$p<0.01$; ***$p<0.005$ (n = 3). Abbreviations: ACACA, Acetyl-CoA Carboxylase Alpha; ACLY, ATP Citrate Lyase; AcCAR, Acetyl-Coenzyme A Carboxylase; ACO2, Aconitase 2; ACSS2, Acyl-CoA Synthetase Short Chain Family; Member 2; ALDOA, aldolase A; ACO2, Aconitase 2; BPG, Bisphosphoglycerate; CPT1, Carnitine Palmitoyltransferase 1; CS, Citrate Synthase; DHCR7, 7-Dehydrocholesterol Reductase; Dnaja3, DnaJ Heat Shock Protein Family (Hsp40) Member A3; FA, Fatty Acid; FADS2, Fatty Acid Desaturase 2; SCD, Stearoyl-CoA Desaturase; FASN, Fatty Acid Synthase; FC, Free Cholesterol; FDFT1, Farnesyl-Diphosphate Farnesyltransferase 1; FDPS, Farnesyl Diphosphate Synthase; FH, Fumarate Hydratase; GOT1, Glutamic-Oxaloacetic Transaminase 1; GLUD1, Glutamate Dehydrogenase 1; GLUL, Glutamate-Ammonia Ligase; HMGCR, 3-Hydroxy-3-Methylglutaryl-CoA Reductase; HMG-CoA, 3-Hydroxy-3-Methylglutaryl-Coenzyme A; IDH1, Isocitrate Dehydrogenase 1; IDH3A, Isocitrate Dehydrogenase 3 (NAD+) Alpha; LDHA, Lactate Dehydrogenase A; MDH2, Malate Dehydrogenase 2; OAA, Oxaloacetic Acid; OGDH, Oxoglutarate (Alpha-Ketoglutarate) Dehydrogenase (Lipoamide); PDHB, Pyruvate Dehydrogenase (Lipoamide) Beta; PEP, Phosphoenolpyruvate; PFKP, Phosphofructokinase, Platelet; ROS, reactive oxygen species; SCD, Stearoyl-CoA Desaturase; SDHA, Succinate Dehydrogenase Complex, Subunit A; SlC27A2, Solute Carrier Family 27 Member 2; SQLE, Squalene Epoxidase; SUCLG1, Succinate-CoA Ligase, Alpha Subunit.

reduction in serum cholesterol levels (Supplemental Figure S16D, http://links.lww.com/HEP/I74). Fatty acid profiling highlighted reduced saturated fatty acid and monounsaturated fatty acid levels in *Dnaja3*-present livers of *Dnaja3*$^{-/-}$ mice (Supplemental Table S18, http://links.lww.com/HEP/I71).

To further investigate the role of *Dnaja3* in NAFLD, we fed male *Dnaja3*$^{-/-}$, *Dnaja3*$^{+/-}$, and *Dnaja3*$^{f/f}$ mice with a high-fat diet (HFD) for 8 weeks, followed by the analysis of liver function (Supplemental Figure S17A, http://links.lww.com/HEP/I75, B, http://links.lww.com/HEP/I75). Interestingly, HFD altered body weight in *Dnaja3*$^{-/-}$ mice (Supplemental Figure S17C, http://links.lww.com/HEP/I75). Comparatively, serum cholesterol, alanine aminotransferase, and aspartate aminotransferase levels in *Dnaja3*$^{-/-}$ mice were significantly higher than in the *Dnaja3*$^{+/-}$, and *Dnaja3*$^{f/f}$ mice under the HFD (Supplemental Figure. S17D–F, http://links.lww.com/HEP/I75). A pronounced elevation in the NASH score and collagen deposition was detected in the liver of *Dnaja3*$^{-/-}$ mice compared to the heterozygous or *Dnaja3*$^{f/f}$ mice on HFD ($p = 0.005$) (Supplemental Figure S17G, http://links.lww.com/HEP/I75). In parallal, the *Dnaja3*$^{-/-}$ mouse livers exhibited a marked increase in apoptosis than *Dnaja3*$^{f/f}$ mice on the same diet (Supplemental Figure S17H, http://links.lww.com/HEP/I75). It is noteworthy to highlight that while *in vivo* observations depicted discernible differences in cell death, the same could not be mirrored in vitro (Supplemental Figure S6E, http://links.lww.com/HEP/I72). Remarkably, the presence of *Dnaja3* in AAV-treated groups resulted in a rescued effect (Supplemental Figure S17D–F, http://links.lww.com/HEP/I75). In conclusion, our rescue experiments utilizing AAV-mediated *Dnaja3* overexpression have provided valuable insights into the role of *Dnaja3* in mitochondrial function and fatty acid metabolism.

DISCUSSION

NASH is associated with obesity, metabolic syndrome, high cholesterol, and type 2 diabetes. Individuals with normal weight could develop metabolic syndrome and abnormal body fat distribution, which are risk factors of NASH and high mortality rates. It is evident that the heritability of body fat distribution is a better diagnostic criterion for the development of NASH rather than body mass index.[14] In this study, we identified a body fat distribution–related rs3747579-TT variant linked to a reduced expression of mitochondrial *DNAJA3* and associated with NASH. Experimentally, *Dnaja3* ablation leads to the development of NASH and HCC in mice with features reminiscent to human NASH and NASH-related HCC. These results are consistent with the hypothesis that individuals carrying a *DNAJA3* variant may have a high risk to develop progressive liver disease.

DNAJA3 collaborates with Hsp70 to bind client proteins, ensuring their proper folding for mitochondrial proteostasis.[31,32] It also acts as a tumor suppressor in solid tumors and plays roles in cell proliferation, survival, and signaling pathways. Its associations with oncogenic proteins and key regulators like HIF-1α and VEGF make it vital in tumorigenesis exploration.[33–35] Moreover, our prior study revealed that full *Dnaja3* knockout leads to early embryonic lethality, with affected embryos dying between E4.5 and E7.5.[36] In this study, *Dnaja3*-deficient cells showed profound loss of mitochondrial structure and severe dysfunction of OXPHOS in *Dnaja3*-deficient cells both *in vivo* and *in vitro*. As a cochaperone, we found that *DNAJA3* interacts with several mitochondrial client proteins, including the mitoribosomal proteins and mitochondrial crucial chaperone, suggesting that *DNAJA3* may provide crucial chaperone activity to mediate mitoribosomal functions for the translation of OXPHOS.

Inhibiting bile acid synthesis leads to cholesterol accumulation, a substrate for bile acid, resulting in liver damage. This accumulation triggers mitochondrial dysfunction, heightening reactive oxygen species production, and fostering fibrogenesis. This cyclical disturbance in hepatic cholesterol and fatty acid homeostasis further accelerates cell death and injury, potentially advancing NASH/HCC progression.[37,38] Together, these insights emphasize DNAJA3's role in NAFLD/NASH pathogenesis and validate our mouse model's representation of the NAFLD to NASH and cirrhosis/HCC continuum, mirroring the human NASH-related HCC progression.

Our study revealed that a metabolic syndrome-related rs3747579-TT variant may serve as the risk allele linked to reduced expression of *DNAJA3* in NASH-related HCC. It is interesting to note that when examining the ALFA Allele Frequency database (https://www.ncbi.nlm.nih.gov/snp/rs3747579#frequency_tab), we found that the rs3747579-TT allele frequency varies among ethnic groups, ranging from 76% (Asian), 72% (European), 58% (Latino), and 21% (African). This coincides with the observation that the NAFLD/NASH prevalence also varies among ethnic groups, ranging from 32% (Middle East), 27% (other Asian), 24% (European), 31% (Latino), and 13% (African).[39] It should be noted that the rs3747579 locus is located approximately 30 kb upstream of *DNAJA3* transcriptional initiation site. While a link between the rs3747579-TT variant and a corresponding reduced expression of *DNAJA3* was validated, the underlying mechanism is unclear. It is known that SNPs in the regulatory regions may have enhancer functions by mediating the binding of critical transcription factors and forming allele-specific long-range chromatin loops with promoters.[40] Future studies should aim to characterize the functional interplay between rs3747579-associated functional SNPs, as well as investigate potential interactions with other transcription factors and chromatin remodeling complexes.

Limitations of the study

First, the number of NASH cases is small in our cohort. It is recognized that genetic studies with confirmed NASH are extremely rare if any because NASH diagnosis requires histological confirmation. Second, we could not analyze obesity and diabetes since these data are not available in the control group. Given the cohort size and limited covariables, this is the limitation of the study, which requires future work to extend this finding.

AUTHOR CONTRIBUTIONS

Ching-Wen Chang, Jeng-Fan Lo, and Xin Wei Wang designed the study, discussed the results, and wrote the manuscript with help from Yu-Syuan Chen, Ching-Wen Chang, and Yu-Syuan Chen performed experiments, and data analysis including all data coordination. Chen-Hua Huang and Chao-Hsiung Lin performed metabolic experiments and data analysis. Wailap Victor Ng and Lichieh Julie Chu performed proteomic experiments and additional bioinformatics analysis. Eric Trépo, Jessica Zucman-Rossi, Kevin Siao, and Jacquelyn J. Maher performed genome study. Men Yee Chiew, Chih-Hung Chou, and Hsien-Da Huang performed RNA-seq experiments and helped with data analysis. Wan-Huai Teo and I-Shan Lee helped with animal experiments. All authors edited and approved the manuscript.

FUNDING INFORMATION

This study was supported by the Ministry of Science and Technology of Taiwan (MOST106-2911-I-010 -513, MOST107-2314-B-010 -024 -MY3, MOST108-2314-B-010-009-MY3, MOST105-2320-B-010-025-MY3, MOST 110-2320-B-A49A-526-MY3 and MOST-111-2811-B-A49A-015), and grants from Ministry of Education, Higher Education of Taiwan SPROUT Project for Cancer Progression Research Center (111W31302) and Cancer and Immunology Research Center (112W31101) to Jeng-Fan Lo, the National Institute of Diabetes and Digestive and Kidney Diseases, National Cancer Institute of the United States (R21DK118380 and P30DK026743) to Jacquelyn J. Maher, and the Intramural Research Program of the Center for Cancer Research, National Cancer Institute of the United States (Z01-BC010313, Z01-BC010876, Z01-BC010877, ZIA-BC011870) to Xin Wei Wang.

ACKNOWLEDGMENT

The authors thank Yao-Kwan Huang for providing electron microscopy services (Institute of Cellular and Organismic Biology, Academia Sinica). We thank Yi-Chen Yeh for helping histological classification of HCC and NASH. The authors also thank the NIH Fellows Editorial Board for editing the manuscript.

CONFLICTS OF INTEREST

Jacquelyn J. Maher consults for BioMarin, Gordian Biosciences, and Myovant. The remaining authors have no conflicts to report.

ORCID

Ching-Wen Chang https://orcid.org/0000–0002–1777–6441
Yu-Syuan Chen https://orcid.org/0000–0002–0658–1040
Chen-Hua Huang https://orcid.org/0000–0003–4681–4256
Chao-Hsiung Lin https://orcid.org/0000–0001–6344–271X
Wailap Victor Ng https://orcid.org/0000–0001–7419–3763
Lichieh Julie Chu https://orcid.org/0000–0002–8488–9614
Eric Trépo https://orcid.org/0000–0003–0475–3934
Jessica Zucman-Rossi https://orcid.org/0000–0002–5687–0334
Jacquelyn J. Maher https://orcid.org/0000–0002–2509–8484
Chih-Hung Chou https://orcid.org/0000–0001–5714–1718
Hsien-Da Huang https://orcid.org/0000–0003–2857–7023
Wan-Huai Teo https://orcid.org/0000–0001–6707–8564
Jeng-Fan Lo https://orcid.org/0000–0001–7188–9140
Xin Wei Wang https://orcid.org/0000–0001–9735–606X

REFERENCES

1. Sung H, Ferlay J, Siegel RL, Laversanne M, Soerjomataram I, Jemal A, et al. Global cancer statistics 2020: GLOBOCAN estimates of incidence and mortality worldwide for 36 cancers in 185 countries. CA Cancer J Clin. 2021;71:209–49.
2. Liu Z, Jiang Y, Yuan H, Fang Q, Cai N, Suo C, et al. The trends in incidence of primary liver cancer caused by specific etiologies: Results from the Global Burden of Disease Study 2016 and implications for liver cancer prevention. J Hepatol. 2019;70:674–83.
3. Huang DQ, El-Serag HB, Loomba R. Global epidemiology of NAFLD-related HCC: Trends, predictions, risk factors and prevention. Nat Rev Gastroenterol Hepatol. 2021;18:223–38.
4. Younossi Z, Anstee QM, Marietti M, Hardy T, Henry L, Eslam M, et al. Global burden of NAFLD and NASH: Trends, predictions, risk factors and prevention. Nat Rev Gastroenterol Hepatol. 2018;15:11–20.
5. Loomba R, Schork N, Chen C-H, Bettencourt R, Bhatt A, Ang B, et al. Heritability of hepatic fibrosis and steatosis based on a prospective twin study. Gastroenterology. 2015;149:1784–93.
6. Caussy C, Soni M, Cui J, Bettencourt R, Schork N, Chen C-H, et al. Nonalcoholic fatty liver disease with cirrhosis increases familial risk for advanced fibrosis. J Clin Invest. 2017;127: 2697–704.

7. Eslam M, George J. Genetic contributions to NAFLD: Leveraging shared genetics to uncover systems biology. Nat Rev Gastroenterol Hepatol. 2020;17:40–52.
8. Kimura M, Iguchi T, Iwasawa K, Dunn A, Thompson WL, Yoneyama Y, et al. En masse organoid phenotyping informs metabolic-associated genetic susceptibility to NASH. Cell. 2022; 185:4216–32 e4216.
9. Mann JP, Anstee QM. NAFLD: PNPLA3 and obesity: A synergistic relationship in NAFLD. Nat Rev Gastroenterol Hepatol. 2017;14:506–7.
10. Leung JCF, Loong TCW, Wei JL, Wong GLH, Chan AWH, Choi PCL, et al. Histological severity and clinical outcomes of nonalcoholic fatty liver disease in nonobese patients. Hepatology. 2017;65:54–64.
11. Pischon T, Boeing H, Hoffmann K, Bergmann M, Schulze MB, Overvad K, et al. General and abdominal adiposity and risk of death in Europe. N Engl J Med . 2008;359:2105–0.
12. Mason C, Craig CL, Katzmarzyk PT. Influence of central and extremity circumferences on all-cause mortality in men and women. Obesity. 2008;16:2690–5.
13. Justice AE, Karaderi T, Highland HM, Young KL, Graff M, Lu Y, et al. Protein-coding variants implicate novel genes related to lipid homeostasis contributing to body-fat distribution. Nat Genet. 2019;51:452–69.
14. Miyake T, Miyazaki M, Yoshida O, Kanzaki S, Nakaguchi H, Nakamura Y, et al. Relationship between body composition and the histology of non-alcoholic fatty liver disease: A cross-sectional study. BMC Gastroenterol. 2021;21:170.
15. Bence KK, Birnbaum MJ. Metabolic drivers of non-alcoholic fatty liver disease. Mol Metab. 2021;50:101143.
16. Florio AA, Campbell PT, Zhang X, Zeleniuch-Jacquotte A, Wactawski-Wende J, Smith-Warner SA, et al. Abdominal and gluteofemoral size and risk of liver cancer: The liver cancer pooling project. Int J Cancer. 2020;147:675–85.
17. Hayashi M, Imanaka-Yoshida K, Yoshida T, Wood M, Fearns C, Tatake RJ, et al. A crucial role of mitochondrial Hsp40 in preventing dilated cardiomyopathy. Nat Med. 2006;12:128–32.
18. Liu J, Tang W, Budhu A, Forgues M, Hernandez MO, Candia J, et al. A viral exposure signature defines early onset of hepatocellular carcinoma. Cell. 2020;182:317–28 e310.
19. Kilkenny C, Browne WJ, Cuthill IC, Emerson M, Altman DG. Improving bioscience research reporting: The ARRIVE guidelines for reporting animal research. PLoS Biol. 2010;8:e1000412.
20. Bale G, Vishnubhotla RV, Mitnala S, Sharma M, Padaki RN, Pawar SC, et al. Whole-exome sequencing identifies a variant in phosphatidylethanolamine N-methyltransferase gene to be associated with lean-nonalcoholic fatty liver disease. J Clin Exp Hepatol. 2019;9:561–8.
21. An X, Liu J, Li Y, Dou Z, Li N, Suo Y, et al. Chemerin/CMKLR1 ameliorates nonalcoholic steatohepatitis by promoting autophagy and alleviating oxidative stress through the JAK2-STAT3 pathway. Peptides. 2021;135:170422.
22. Anstee QM, Darlay R, Cockell S, Meroni M, Govaere O, Tiniakos D, et al. Genome-wide association study of non-alcoholic fatty liver and steatohepatitis in a histologically characterised cohort. J Hepatol. 2020;73:505–15.
23. Thul PJ, Lindskog C. The human protein atlas: A spatial map of the human proteome. Protein Sci. 2018;27:233–44.
24. Barretina J, Caponigro G, Stransky N, Venkatesan K, Margolin AA, Kim S, et al. The Cancer Cell Line Encyclopedia enables predictive modelling of anticancer drug sensitivity. Nature. 2012; 483:603–7.
25. Paterson HAB, Yu S, Artigas N, Prado MA, Haberman N, Wang YF, et al. Liver RBFOX2 regulates cholesterol homeostasis via Scarb1 alternative splicing in mice. Nat Metab. 2022;4:1812–29.
26. Sakurai T, He G, Matsuzawa A, Yu GY, Maeda S, Hardiman G, et al. Hepatocyte necrosis induced by oxidative stress and IL-1 alpha release mediate carcinogen-induced compensatory proliferation and liver tumorigenesis. Cancer Cell. 2008;14:156–65.
27. Schuster S, Cabrera D, Arrese M, Feldstein AE. Triggering and resolution of inflammation in NASH. Nat Rev Gastroenterol Hepatol. 2018;15:349–64.
28. Chang CW, Chen YS, Tsay YG, Han CL, Chen YJ, Yang CC, et al. ROS-independent ER stress-mediated NRF2 activation promotes warburg effect to maintain stemness-associated properties of cancer-initiating cells. Cell Death Dis. 2018;9:194.
29. Chang CW, Chen YS, Chou SH, Han CL, Chen YJ, Yang CC, et al. Distinct subpopulations of head and neck cancer cells with different levels of intracellular reactive oxygen species exhibit diverse stemness, proliferation, and chemosensitivity. Cancer Res. 2014;74:6291–305.
30. Wang W, Liu X, Wei P, Ye F, Chen Y, Shi L, et al. SPP1 and CXCL9 promote non-alcoholic steatohepatitis progression based on bioinformatics analysis and experimental studies. Front Med (Lausanne). 2022;9:862278.
31. Lu B, Garrido N, Spelbrink JN, Suzuki CK. Tid1 isoforms are mitochondrial DnaJ-like chaperones with unique carboxyl termini that determine cytosolic fate. J Biol Chem. 2006;281:13150–58.
32. Sayson SL, Fan JN, Ku CL, Lo JF, Chou SH. DNAJA3 regulates B cell development and immune function. Biomed J. 2023: 100628. doi:10.1016/j.bj.2023.100628
33. Chen YS, Chang CW, Tsay YG, Huang LY, Wu YC, Cheng LH, et al. HSP40 co-chaperone protein Tid1 suppresses metastasis of head and neck cancer by inhibiting Galectin-7-TCF3-MMP9 axis signaling. Theranostics. 2018;8:3841–55.
34. Chen CY, Chiou SH, Huang CY, Jan CI, Lin SC, Hu WY, et al. Tid1 functions as a tumour suppressor in head and neck squamous cell carcinoma. J Pathol. 2009;219:347–55.
35. Chen CY, Jan CI, Lo JF, Yang SC, Chang YL, Pan SH, et al. Tid1-L inhibits EGFR signaling in lung adenocarcinoma by enhancing EGFR Ubiquitinylation and degradation. Cancer Res. 2013;73:4009–19.
36. Lo JF, Hayashi M, Woo-Kim S, Tian B, Huang JF, Fearns C, et al. Tid1, a cochaperone of the heat shock 70 protein and the mammalian counterpart of the Drosophila tumor suppressor l(2) tid, is critical for early embryonic development and cell survival. Mol Cell Biol. 2004;24:2226–36.
37. Ioannou GN. The role of cholesterol in the pathogenesis of NASH. Trends Endocrinol Metab. 2016;27:84–95.
38. Arguello G, Balboa E, Arrese M, Zanlungo S. Recent insights on the role of cholesterol in non-alcoholic fatty liver disease. Biochim Biophys Acta. 2015;1852:1765–78.
39. Younossi Z, Tacke F, Arrese M, Chander Sharma B, Mostafa I, Bugianesi E, et al. Global perspectives on nonalcoholic fatty liver disease and nonalcoholic steatohepatitis. Hepatology. 2019;69: 2672–82.
40. Tian J, Lou J, Cai Y, Rao M, Lu Z, Zhu Y, et al. Risk SNP-mediated enhancer-promoter interaction drives colorectal cancer through both FADS2 and AP002754.2. Cancer Res. 2020;80: 1804–18.

How to cite this article: Chang C, Chen Y, Huang C, Lin C, Ng WV, Chu LJ, et al. A genetic basis of mitochondrial *DNAJA3* in nonalcoholic steatohepatitis-related hepatocellular carcinoma. Hepatology. 2025;81:60–76. https://doi.org/10.1097/HEP.0000000000000637